Tellus (1987), *39A*, 25–32

A modified time-longitude diagram applied to 500 mb heights along 50° north and south

By KLAUS FRAEDRICH* and MARTIN LUTZ, *Institut für Meteorologie, Freie Universität Berlin, D-1000 Berlin 41, F.R. Germany*

(Manuscript received November 21, 1985; in final form May 5, 1986)

ABSTRACT

The common time-longitude section (or Hovmöller diagram) shows longitude and intensity of troughs and ridges as a function of time. It is modified to a time-longitude lag-correlation diagram to yield statistically relevant estimates of zonal wavelengths, phase and group velocities. Different scales can be distinguished after the data sets have been treated by band- and low-pass filters. The lag-correlation analysis is applied to the 500 mb geopotential height along 50°N and 50°S for individual basepoints and averaged over the latitude circle. This technique is also useful if the local or zonally averaged dynamics of numerical models is to be statistically verified.

1. Introduction

Longitude-time sections of meteorological variables reveal zonal displacements of atmospheric processes. Since the early 1940's, such diagrams have been used to deduce the phase propagation of troughs and ridges and, subsequently, to extrapolate the motion of centers of action (Rossby and Collaborators, 1939; Namias and Clapp, 1944; Cressman, 1948). The concept of energy propagation, as evidenced by increasing amplitudes of ridges and troughs, has been introduced to meteorology by Rossby (1945, Fig. 2). His ideas have been pursued by Hovmöller (1949), who published the first quantitative application of downstream intensification of synoptic systems in a time-longitude section (the "Hovmöller diagram"). Recently the concept of Rossby wave energy dispersion used its relevance to atmospheric planetary waves (on a sphere) has become widely recognized (e.g., Hoskins et al., 1977), because it appears to be applicable to the dispersion of the low-frequency variability observed in both hemispheres. Thus the Hovmöller diagram should be revisited and modified to provide statistically relevant estimates of wavelength, phase and group velocities of various scales of motion.

Hovmöller (1949) constructed a trough-ridge diagram as a time-longitude matrix of daily 500 mb geopotential heights on a latitude circle (or using an average over 25° latitude) in the belt of the northern hemispheric westerlies. From such a diagram, he was able to estimate wavelength, phase and group velocity of zonal waves for an individual month (November, 1945) in order to evaluate the Rossby dispersion relation. From the slopes of successive maximum trough and ridge development, he determined the group velocity; the phase velocity is characterized by the progression (or retrogression) of an individual ridge or trough. Such diagrams have also been constructed for the southern hemisphere geopotential height fields of the midlatitude westerlies (Van Loon, 1965) and, using satellite pictures, for cloud cluster disturbances in the tropical easterlies (Chang, 1970). However, only individual trough and ridge systems can be traced by this method so that it is difficult to obtain statistical estimates in terms of seasonal averages or selected scales of disturbances. Furthermore, intensity changes and

* On leave at the Bureau of Meteorology Research Centre, Melbourne, Australia.

phase propagation properties of individual systems are often blurred by noise or random perturbations which need to be averaged out. Therefore we suggest in this note to modify Hovmöller's original trough-ridge diagram to a longitude-time lag-correlation diagram which includes both time and longitudinal lags. Furthermore, time filters are applied to the data set to distinguish different scales of disturbances.

In the following note, the method of analysis is described in Section 2 which includes an estimate of the significance of the correlation coefficients. An application to the 500 mb geopotential along 50°N is presented in Section 3, along 50°S in Section 4.

2. Data and methods of analysis

Daily geopotential height profiles $z(\lambda, t)$ of 15 winter seasons (1967/68 to 1981/82) are gridded on a 10° longitude grid (λ) along the latitude circle of 50°N. The zonal scale of the smallest eddy resolved will be 1430 km. The data sets have equal length of 120 days beginning on 1 November. The annual cycle is removed from each gridpoint

$$z(\lambda, t) = \text{removed} + z^*(\lambda, t) \tag{2.1}$$

by the annual harmonic of the 15-year period of observations. The remaining deviations $z^*(\lambda, t)$ are statistically analysed in the following. To distinguish representative scales, geopotential height anomalies $z^*(\lambda, t)$ are subjected to time filtering before correlation coefficients are derived. Common band- and low-pass filters are applied (Blackmon, 1976) using 31 weighting points. This reduces the unfiltered 120 day season by the first and the last 15 days, i.e., the filtered seasons consist of 90 days. The band-pass filter responds to periods between 5 and 10 days. The low-pass filtered data contain periods longer than 15 days. These filters were arbitrarily chosen to demonstrate the technique.

2.1. *Zonal-time lag-correlations*

Correlation coefficients are determined from the unfiltered, band- and low-pass filtered geopotential height anomalies z^* of zonal gridpoints centered on the basepoint at longitude λ:

$$r(\lambda, m\Delta\lambda, n\Delta t) = \frac{\operatorname{cov}(z^*(\lambda, t), z^*(\lambda + m\Delta\lambda, t + n\Delta t))}{[\operatorname{var} z^*(\lambda, t) \operatorname{var} z^*(\lambda + m\Delta\lambda, t)]^{1/2}}. \tag{2.2}$$

Zonal lags $m\Delta\lambda$ refer to multiples m of $\Delta\lambda = 10°$ longitude eastward of the basepoint λ along the 50°N latitude circle; time lags $n\Delta t$ are multiples n of the sampling time $\Delta t = 1$ day. It should be noted that $\operatorname{var} z^*(\lambda, t) \neq \operatorname{var} z^*(\lambda + m\Delta\lambda, t)$ but $\operatorname{var} z^*(\lambda + m\Delta\lambda, \ t) \doteq \operatorname{var} z^*(\lambda + m\Delta\lambda, \ t + n\Delta t)$. Thus one obtains for each base point λ:

(i) Simultaneous correlations $r(\lambda, m\Delta\lambda, n = 0)$, which lead to a zonal profile of m coefficients; they depend on $m = 0, \ldots, 36$ space steps which are a zonal distance of $\Delta\lambda = 10°$ longitude apart.

(ii) An autocorrelation profile $r(\lambda, m = 0, n\Delta t)$ of n correlation coefficients; they depend on $n + 1$ time steps which are a sampling time $\Delta t = 1$ day apart.

(iii) A zonal-time lag-correlation matrix leads to the modified Hovmöller diagram of $m \times n$ correlation coefficients $r(\lambda, m\Delta\lambda, n\Delta t)$ displayed in zonal-time lag coordinates $(m\Delta\lambda, n\Delta t)$ with an $(\lambda + m\Delta\lambda)$-abscissa and $(n\Delta t)$-ordinate centered at the basepoint λ and zero time-lag $n = 0$. The coefficients of the simultaneous correlations $r(\lambda, m\Delta\lambda, n = 0)$ occur on the abscissa at $n = 0$, the autocorrelations appear on the ordinate at $m = 0$.

An example (Fig. 1) of the modified time-longitude diagram is shown for a wave group which consists of two waves of equal amplitude but slightly different wavelengths. Their wavenumbers $k + \Delta k$, $k - \Delta k$ and the related frequencies $v + \Delta v$, $v - \Delta v$ differ by $2\Delta k$ and $2\Delta v$, respectively. The resulting wavegroup (e.g., Holton, 1979):

$$z^*(\lambda, t) = 2 \cos(\Delta k\lambda - \Delta v t) \cos(k\lambda - vt) \tag{2.3}$$

consists of a lower frequency ($\Delta v = 0.08$ d^{-1}) envelope with a zonal wavelength $\Delta l = 2\pi/\Delta k$, 360° longitude, and a higher frequency ($v = 0.13$ d^{-1}) carrier wave of the wavelength $l = 2\pi/k$, 72° longitude. The carrier wave progresses with the phase velocity

$$c_p = \frac{v}{k},$$

which represents an average of the two wave components ($c_p \sim 10°$ per day). The zonal-time lag-correlation diagram (Fig. 1) reveals the phase speed by the slope of maximum positive or

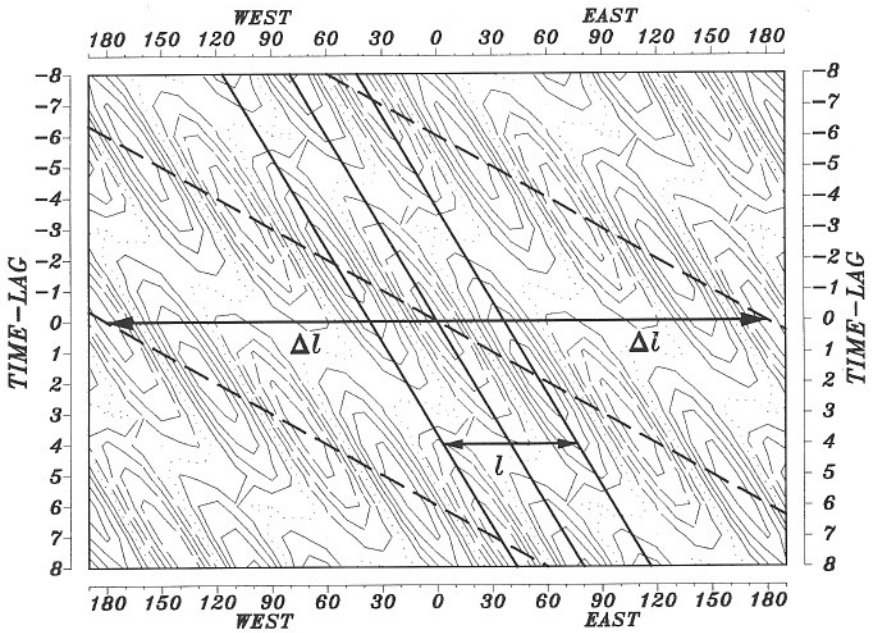

Fig. 1. Time-longitude lag-correlation diagram for a theoretical wavegroup centered at the basepoint $\lambda = 0°$. The phase velocity of the carrier wave is determined by the slope of the full line, its wavelength is given by twice the zonal distance between neighbouring lines. The group velocity (of the wave envelope) is represented by the slope of the dashed line, its wavelength by doubling the zonal distance between two adjacent lines.

negative correlation coefficients (full line). The related wavelength l is twice the distance (on the abscissa $n = 0$) between maximum and minimum correlation coefficients. The zonal group velocity

$$c_g = \frac{\Delta v}{\Delta k} \qquad \text{with } \Delta k \to 0$$

defines the progression of the lower frequency envelope ($c_g \sim 30°$/day). It is given by the slope of the (dashed) line which connects the correlation maximum in the center (surrounded by dashed contours) with the neighbouring correlation minima (surrounded by full contours) related to positive and negative time lags. The related wavelength Δl is twice the distance (on the abscissa $n = 0$) between these two sloping lines of neighbouring maximum and minimum correlation coefficients. For comparison the common trough-ridge diagram may also be constructed. The phase or group velocities of the theoretical wavepacket (2.3) can be verified, if one follows the maximum positive (or negative) amplitudes or connects alternating maxima and minima. For an idealized wavegroup the structures of the longitude-time section are identical with those of the lag-correlation diagram; the latter is centered at the basepoint with zero time lag.

2.2. *Time scales and significance*

Autocorrelations $r(\lambda, m = 0, n\Delta t)$ determine the time lag correlation profiles at each gridpoint λ. They allow an estimate of a time scale which denotes the time between effectively independent observations. Referring to correlations between the time series $z^*(\lambda, t)$ and $z^*(\lambda + m\Delta\lambda, t)$ a time scale (Bartlett, 1935, see also Trenberth, 1984, for some details) is defined for all pairs of gridpoints $(\lambda, \lambda + m\Delta\lambda)$:

$$T_0(\lambda, m\Delta\lambda) = 1 + 2 \sum_{n=1}^{N} (1 - n/N) r(\lambda, m = 0, n\Delta t) \times r(\lambda + m\Delta\lambda, m = 0, n\Delta t). \qquad (2.4)$$

Assuming red noise, i.e., a first order autoregressive process (AR), the autocorrelations at the basepoints λ and $\lambda + m\Delta\lambda$ for a lag n are estimated by $r(n) = r^n(\lambda, m = 0, n = 1)$, i.e., they decay with the nth power of the lag-one autocorrelation. Other more realistic models, e.g., autoregressive moving average processes (ARMA) may be used instead, as suggested by

Thiebeaux and Zwiers (1984) or Fraedrich and Dümmel (1983) applying an information criterion for order termination. It should be noted that autoregressive (AR) processes fit the data as well as ARMA processes; one may even use a less time consuming procedure and determine a zonally averaged integral or macro-time scale as evaluated by Stefanick (1981) and Kietzig (1984) and suggested by Leith (1982) for estimating the time scale related to variance (note the factor $\frac{1}{2}$ which is involved).

Averaging the correlation time scale matrix based on red noise, $T_0(\lambda, m\Delta\lambda)$, gives a representative mean value $\overline{T}_0$ for the 50° N latitude circle. For the unfiltered, band-, and low-pass filtered data sets one obtains the following mean time scales as averages over 36×36 T_0's:

$\overline{T}_0 = (3.2; 1.9; 19.2)$ days for winter.

The observed max $T_0 = (4.1, 2.1, 20.9)$ days and min $T_0 = (2.2, 1.7, 18.1)$ days reveal only minor deviations from the mean $\overline{T}_0$. To evaluate the significance of the correlation coefficients the appropriate degrees of freedom are defined by independent data, i.e., the number of observations is reduced by the factor sampling time Δt/time scale T_0.

It should be noted that every correlation coefficient $r(\lambda, m\Delta\lambda, n\Delta t)$ is related with its correlation time scale $T_0(\lambda, m\Delta\lambda)$, if the degrees of freedom are evaluated for the significance test. For practical purposes, however, the level of significant correlation coefficients does not vary if the same $\overline{T}_0$ or max T_0 is used for all pairs of correlated time series, because the difference is small; max T_0 would place the level of significance on the safe side. Thus one obtains the following 10% significant correlation coefficients for the unfiltered (r_u), band- (r_b), and low-pass filtered (r_l) data sets: $r_u = 0.08$, $r_b = 0.07$, $r_l = 0.21$. For zonally averaged correlation coefficients, one finds: $r_u = 0.013$, $r_b = 0.011$, $r_l = 0.035$.

3. Time-longitude lag-correlations for 50° N

In Hovmöller's method geopotential heights of the 500 mb surface along a latitude circle are plotted on the horizontal axis (abscissa) and time increases downward (coordinate). Longitude-time lag-correlation diagrams are centered at a basepoint λ; longitude lags increase eastward and time lags increase downward. These diagrams display phase speeds, group velocities and the associated wavelengths (as shown in Fig. 1 for a

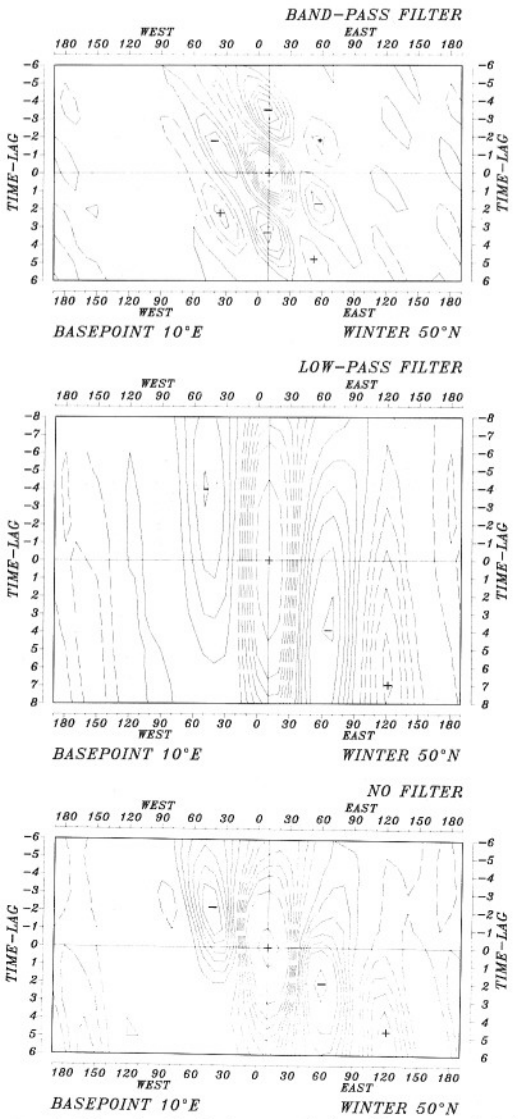

Fig. 2. Time-longitude lag-correlation diagrams of the 500 mb geopotential height deviations along 50° N for 15 winter seasons centered at basepoint $\lambda = 10°$ E. Positive, negative and zero correlation coefficients are plotted by dashed, full and dotted contours. There is equal spacing of the lag-correlation isolines starting from zero in 0.1 (0.05) steps for filtered (unfiltered) data sets; $r = 0.8$ is the contour about the basepoint. From top to bottom: band-pass (a) and low-pass (b) filtered, and unfiltered data (c).

theoretical wavepacket) which characterize the situation around a selected basepoint. In this section, diagrams are constructed for unfiltered, band- and low-pass filtered 500 mb heights along 50°N, which are centered at the selected basepoint at $\lambda = 10°$E (Figs. 2a–c) and averaged over all (36) individual basepoints (zonal mean, Figs. 3a–c). This and other individual gridpoints reveal lag-correlation patterns similar to the zonal average, which will be discussed in more detail. The only exceptions are low-pass filtered analyses at individual basepoints, because in the northern hemisphere the long-period disturbances are zonally asymmetric and characterized by group velocities varying along the latitude circle. Furthermore it should be noted that the unfiltered data set shows a lag one-day correlation of greater than 0.7 at 10°E (Fig. 2c), which is in agreement with Gutzler and Mo (1983).

The band-pass filtered height deviations lead to a zonal mean longitude-time lag-correlation diagram which is shown in Fig. 3a. One observes a phase speed $c_p \sim 10°$ per day, which is given by the slope of the maximum positive or negative correlation coefficients. This value is slightly smaller than the phase speed of 12.5° per day, which can be deduced from Blackmon et al. (1984, Fig. 1); this is due to the longer periods passing our band-pass filter. The related zonal wavelength of about 60° longitude (wavenumber $k = 6$) can be estimated by the distance between two minima of the simultaneous correlation coefficients, i.e., along the abscissa $n = 0$. The zonal group velocity $c_g \sim 30$ to 35°/day is determined by the slope of the line which connects the correlation maximum in the center (surrounded by dashed contours) with the neighbouring minima (surrounded by full contours) related to positive and negative time lags. Furthermore, there is an indication of a wavelength of about 240° longitude ($k \sim 1.5$), which may be interpreted as the envelope for the wavegroup.

The low-pass filtered longitude-time lag-correlation diagram (zonally averaged over all gridpoints, Fig. 3b) shows a stationary wavetrain with a wavelength of about 110 to 120° longitude (wavenumber $k \sim 3$). The wavepacket encounters a group velocity $c_g \sim 22.5°$ per day eastward. This can be estimated if one follows the series of correlation extrema which alternate their sign when changing from negative to positive time lags. This pattern can be identified for about 2 wavelengths. These wavegroups seem to resemble the wavetrains discussed by Blackmon et al.

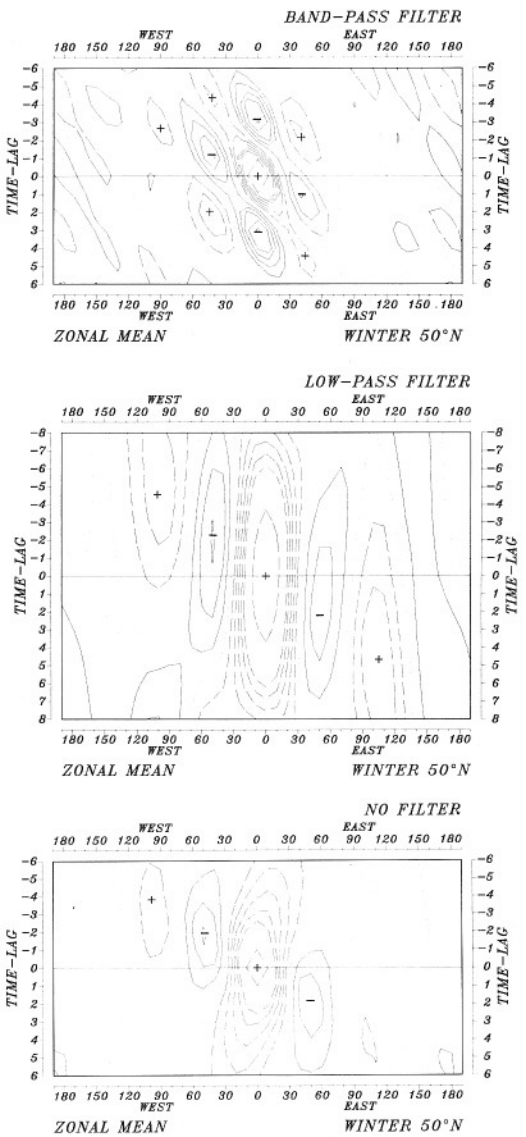

Fig. 3. Zonally averaged time-longitude lag-correlation diagrams of the 500 mb geopotential height deviations along 50°N for 15 winter seasons. Positive, negative and zero correlation coefficients are plotted by dashed, full and dotted contours. There is equal spacing of the lag-correlation isolines starting from zero in 0.005 steps; $r = 0.05$ is the contour about the basepoint. From top to bottom: band-pass (a) and low-pass (b) filtered, and unfiltered data (c).

(1984) associated with the 10- to 30-day time scale. They are organized in more zonally oriented waveguides originating in the jet entrance regions, retain their shape and simply translate eastward with the basepoint. However, further studies are necessary to fully explore the underlying dynamics. The unfiltered zonally averaged longitude-time lag-correlation diagram (Fig. 3c) shows also a stationary wavetrain and the structures can hardly be distinguished from the low-pass filtered patterns, i.e., most of the variance of the northern hemisphere westerlies is contributed by the long-period fluctuations.

From the graphs in Fig. 1 to 3, it is obvious that the waves and their propagation properties are determined by the positive and negative maxima of the correlation coefficients. Therefore their significance needs to be tested: All maxima and secondary minima (in Figs. 2, 3) are significant on the 10% level (see Section 2). The only exceptions are the secondary minima occurring in the zonally averaged low-pass filtered correlation matrix (Fig. 3b) because the long-period processes are zonally asymmetric.

4. Time-longitude lag-correlations for 50°S

The analysis is also applied to daily 500 mb geopotential height profiles $z(\lambda, t)$ of 5 winter seasons (1960–64) gridded on a 10° longitude grid along 50°S. The data sets have an equal length of 120 days beginning on 1 May. The annual cycle is removed from each grid point by fitting a least squares parabola to the five winter seasons. The remaining deviations $z^*(\lambda, t)$ are statistically analysed. The filters applied are the same as those used for the 50°N latitude circle. The unfiltered, band-, and low-pass filtered data sets yield the following average time scales (Subsection 2.2):

$\overline{T}_0 = (1.7; 1.8; 18.8)$ days for winter.

The observed max $T_0 = (3.5; 2.7; 20.1)$ days and min $T_0 = (1.2; 1.5; 16.7)$ reveal small deviations from the mean. Reducing the number of observations by the factor sampling time Δt/time scale T_0 leads to the appropriate degrees of freedom which enter the significance test. The following 10% significant zonally averaged correlation coefficients are obtained for the unfiltered (r_u), band- (r_b), and low-pass filtered (r_l) data sets

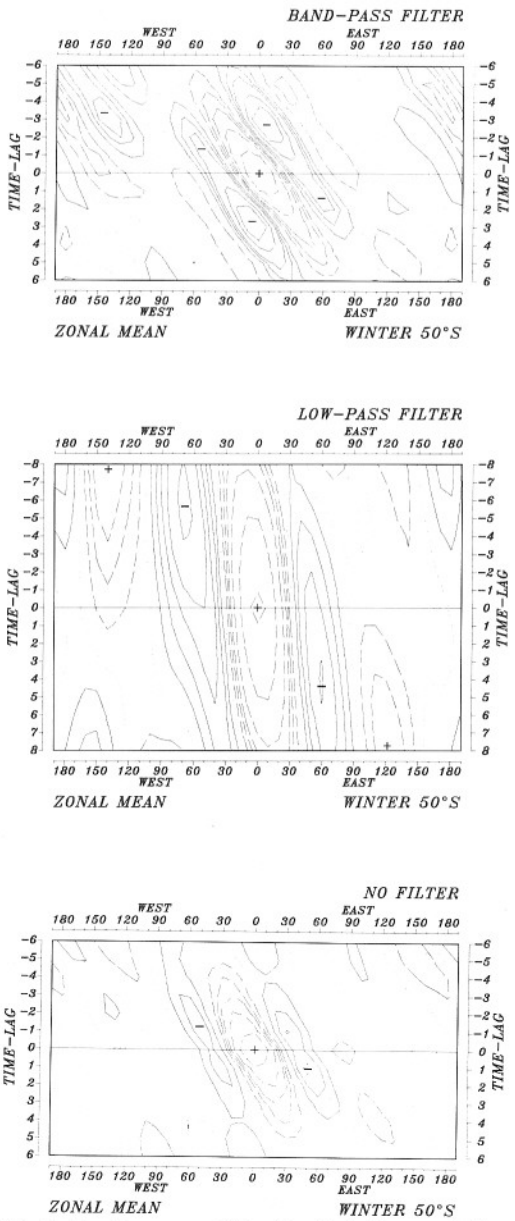

Fig. 4. Zonally averaged time-longitude lag-correlation diagrams of the 500 mb geopotential height deviations along 50°S for 5 winter seasons. Positive, negative and zero correlation coefficients are plotted by dashed, full and dotted contours. There is equal spacing of 0.01 steps for low-pass filtered correlations with $r = 0.1$ about the basepoint; contours for unfiltered and band-pass filtered correlations are 0.01, 0.02, 0.03, 0.05, 0.1. From top to bottom: band-pass (a) and low-pass filtered (b) and unfiltered (c) data.

along 50°S: $r_u = 0.021$, $r_b = 0.021$, $r_l = 0.058$; they are based on max T_0 values.

The band-pass and unfiltered lag-correlations reveal similar patterns for many basepoints and the zonal average (Figs. 4a, c). They show a zonal wavelength of 70° to 80° longitude measured between every second zero-correlation contour on the abscissa ($n = 0$) or by the distance of two minima of simultaneous correlations. The zonal phase speed $c_p \sim 10°$/day is determined by the slope of the maximum positive or negative correlation coefficients. The zonal group velocity $c_g \sim 40$ to 50°/day is defined by the slope of the line which connects the correlation maximum in the center with the neighbouring correlation minima related to positive and negative time lags. A non-divergent Rossby wave of the same wavelength, phase and group velocity ($c_{p,g} = u \mp \beta k^{-2}$) would require a zonal current of $u \sim 27.5$ to 32.5°/day or $u \sim 22.5$ m/s, which is in agreement with observed climatological mean values for winter (Trenberth, 1982, Fig. 1). In the low-pass filtered lag-correlation diagram one observes a quasi-stationary wave train with a wavelength of 110° longitude; Fig. 4b suggests $c_p \sim 2°$/day as phase velocity. The wave packet is characterized by a group velocity of $c_g \sim 12°$/day. The 50°N analysis (Figs. 3b, c) shows strong similarity of unfiltered and low-pass filtered lag-correlation diagrams indicating that most of the variance is contributed by quasi-stationary long period fluctuations (Section 3). In the southern hemisphere, however, eastward propagating shorter period disturbances provide most of the variance (Fraedrich and Kietzig, 1983), which leads to the observed similarity between band-pass and unfiltered lag-correlations.

All maxima and secondary minima of the correlation coefficients are significant on the 10% level. The only exceptions are the secondary minima occurring in the low-pass filtered correlation matrix (Fig. 4b).

5. Conclusion

This study introduces a modification of the Hovmöller trough-and-ridge diagram in terms of longitude-time lag-correlations to obtain statistically relevant estimates of zonal wavelengths, phase and group velocities of disturbances in the atmospheric circulation. Time filters can be applied to the data set to distinguish different scales of disturbances. The statistics can be evaluated for the zonal environment of an individual gridpoint or in a zonally averaged sense. Applications to the 500 mb geopotential heights along 50°N and 50°S lead to estimates for short period fluctuations (band-pass filtered geopotentials) which are related to synoptic disturbances, and the long period variations of quasi-stationary processes. Besides the relevance for analysing empirical data these lag-correlation techniques provide a method to verify model outputs (locally and in a zonally averaged sense) by estimating and testing the statistical properties of various scales of motion. Furthermore, lag-correlation maps give local informations, which cannot be obtained from common wavenumber-frequency analyses (e.g., Fraedrich and Böttger, 1978).

6. Acknowledgements

Discussions with J. M. Wallace lead to this paper. Thanks are due to Ms. M. Scholz for preparing the manuscript; referees' comments are appreciated.

REFERENCES

Bartlett, M. S. 1935. Some aspects of the time-correlation problem in regard to tests of significance. *J. R. Stat. Soc. 98*, (New Series, part 3), 536–543.

Blackmon, M. L. 1976. A climatological spectral study of the 500 mb geopotential height of the Northern Hemisphere. *J. Atmos. Sci. 33*, 1607–1623.

Blackmon, M. L., Lee, Y.-H., Wallace, J. M. and Hsu, H.-H. 1984. Time variation of 500 mb height fluctuations with long, intermediate and short time scales as deduced from lag-correlation statistics. *J. Atmos. Sci. 41*, 981–991.

Cressman, G. P. 1948. On the forecasting of long waves in the upper westerlies. *J. Meteorol. 5*, 44–57.

Chang, C. P. 1970. Westward propagating cloud

patterns in the tropical Pacific as seen from time-composite satellite photographs. *J. Atmos. Sci. 27*, 133–138.

Fraedrich, K. and Böttger, H. 1978. A wavenumber-frequency analysis of the 500 mbar geopotential at 50° N. *J. Atmos. Sci. 35*, 745–750.

Fraedrich, K. and Dümmel, Th. 1983. On single station forecasting: the geopotential height, its vertical and time structure and 500 mbar ARMA prediction. *Contrib. Atmos. Phys. 56*, 221–239.

Fraedrich, K. and Kietzig, E. 1983. Statistical analysis and wavenumber-frequency spectra of the 500 mb geopotential along 50°S. *J. Atmos. Sci. 40*, 1037–1045.

Gutzler, D. S. and Mo, K. C. 1983. Autocorrelation of Northern Hemisphere geopotential heights. *Mon. Wea. Rev. 111*, 155–164.

Holton, J. R. 1979. *An introduction to dynamic meteorology*. Acad. Press, 391 pp.

Hoskins, B. J., Simmons, A. J. and Andrews, D. S. 1977. Energy dispersion in a barotropic atmosphere. *Q. J. R. Meteorol. Soc. 103*, 553–567.

Hovmöller, E. 1949. The trough-and-ridge diagram. *Tellus 1*(2), 62–66.

Kietzig, E. 1984. Statistical analysis of the 500 mb geopotential along 50° north and south: moments and time scales. *Meteorol. Rdsch. 37*, 111–116.

Leith, C. E. 1982. Statistical methods for the verification of long and short range forecasts. Seminar 1981—Problems and prospects in long and medium range weather forecasting. European Centre for Medium Range Weather Forecasts, 313–335.

Namias, J. and Clapp, P. F. 1944. Studies in the motion and development of long waves in the westerlies. *J. Meteorol. 1*, 57–77.

Rossby, C.-G. and Collaborators, 1939. Relation between variations in the intensity of the zonal circulation of the atmosphere and the displacement of the semipermanent centers of action. *J. Marine Res. 2*, 38–55.

Rossby, C.-G. 1945. On the propagation of frequencies and energy in certain types of oceanic and atmospheric waves. *J. Meteorol. 2*, 187–204.

Stefanick, M. 1981. Space and time scales of atmospheric variability. *J. Atmos. Sci. 38*, 988–1002.

Thiebaux, H. J. and Zwiers, F. W. 1984. The interpretation and estimation of effective sample size. *J. Clim. Appl. Meteorol. 23*, 800–811.

Trenberth, K. E. 1982. Seasonality in Southern Hemisphere eddy statistics at 500 mb. *J. Atmos. Sci. 39*, 2507–2520.

Trenberth, K. E. 1984. Some effects of finite sample size and persistence on meteorological statistics. Part I: Autocorrelations. *Mon. Wea. Rev. 112*, 2359–2368.

van Loon, H. 1965. A climatological study of the atmospheric circulation in the Southern Hemisphere during IGY. Part 1. *J. Appl. Meteorol. 4*, 479–491.